Multiple-scale thermo-acoustic stability analysis of a coaxial jet combustor

L. Magri[a,d], Y.-C. See[b], O. Tammisola[c], M. Ihme[a], M.P. Juniper[d]

[a] *Center for Turbulence Research, Stanford University, 488 Escondido Mall, Stanford, CA 94305, USA*
[b] *Convergent Science, Madison, WI 53719, USA*
[c] *Mechanical, Materials and Manufacturing Engineering, University of Nottingham, Nottingham, NG7 2RD, UK*
[d] *Cambridge University Engineering Department, Trumpington Street, Cambridge, CB2 1PZ, UK*

Abstract

In this paper, asymptotic multiple-scale methods are used to formulate a mathematically consistent set of thermo-acoustic equations in the low-Mach number limit for linear stability analysis. The resulting sets of nonlinear equations for hydrodynamics and acoustics are two-way coupled. The coupling strength depends on which multiple scales are used. The double-time-double-space (2T-2S), double-time-single-space (2T-1S) and single-time-double-space (1T-2S) limits are revisited, derived and linearized. It is shown that only the 1T-2S limit produces a two-way coupled linearized system. Therefore this limit is adopted and implemented in a finite-element solver. The methodology is applied to a coaxial jet combustor. By using an adjoint method and introducing the intrinsic sensitivity, (i) the interaction between the acoustic and hydrodynamic subsystems is calculated and (ii) the role of the global acceleration term, which is the coupling term from the acoustics to the hydrodynamics, is analysed. For the confined coaxial jet diffusion flame studied here, (i) the growth rate of the thermo-acoustic oscillations is found to be more sensitive to small changes in the hydrodynamic field around the flame and (ii) increasing the global acceleration term is found to be stabilizing in agreement with the Rayleigh Criterion.

Keywords: Thermo-acoustics, Stability, Adjoint methods, Multiple-scale analysis, Sensitivity analysis

1. Introduction

Thermo-acoustic oscillations in gas turbines and rocket engines can lead to catastrophic failure and are one of the most persistent problems facing engine manufacturers [1]. They arise when acoustic pressure fluctuations occur sufficiently in phase with heat-release fluctuations. This converts thermal energy to mechanical energy over a cycle [2].

Thermo-acoustic oscillations are governed by the interaction between two macro subsystems: the combusting hydrodynamics and the acoustics. The hydrodynamics determines the flow field around the flame. The acoustics excites hydrodynamic structures at the flame base, which are then convected downstream, causing heat-release fluctuations. Although it has been argued that hydrodynamic instability has little influence on the thermo-acoustic stability, experiments [3] showed that the frequency of the coupled hydrodynamic/thermo-acoustic system is dictated by the hydrodynamic mechanism at some operating con-

Email address: lmagri@stanford.edu (L. Magri)

ditions and the thermo-acoustic mechanism at others. The interactions between the two subsystems is still not fully understood.

Linear stability analysis is often used to predict whether a combustion system will experience thermo-acoustic oscillations. The hydrodynamic subsystem is typically modelled by a response function [e.g. 4, 5], or a time-delayed model [e.g. 1], relating the heat release to the acoustic velocity. These models are coupled with low-order acoustic solvers, such as network models or Helmholtz solvers [6], and the eigenvalues are calculated. If at least one eigenvalue has positive growth rate, the system is unstable. The sensitivity of the stability to external feedback mechanisms or passive control has been calculated with adjoint-based methods [7, 8, 9], which were recently experimentally validated [10]. However, these versatile methods were applied only to simplified thermo-acoustic models with uniform mean flows.

In most thermo-acoustic models, the interaction from the acoustics to the hydrodynamics is globally simulated by a simplified convection model, such as the $n - \tau$ model, meaning that the hydrodynamic variables are not included in the state vector. The system is only one-way coupled. To overcome this limitation, multiple-scale methods were applied by Moeck et al. [11], Mariappan and Sujith [12], Balaji and Chakravarthy [13] to capture the two-way interaction between the hydrodynamics and acoustics. Moeck et al. [11] used one time and two spatial scales (1T-2S) to couple a one-dimensional acoustic network model with a one-dimensional low-Mach number flame solver. Using the same multiple scales, Mariappan and Sujith [12] studied the nonlinearities in an electrical Rijke-tube with one-dimensional acoustics. The effect that the acoustics has on the hydrodynamics was assumed to be uniform in the hydrodynamic domain. Balaji and Chakravarthy [13] used two time and two spatial scales (2T-2S) in nonlinear simulations of a backward-facing step diffusion flame combustor to investigate the role of the acoustic Reynolds stress.

The main contribution of this paper is to develop and apply a three-dimensional thermo-acoustic linear model able to capture the two-way coupling between the hydrodynamics and acoustics. We apply the method to an axisymmetric coaxial jet combustor [14, 15, 16] with a diffusion flame. The chemistry is modelled by a one-step reaction but could be extended to detailed chemistry models. The *intrinsic sensitivity* is calculated with an adjoint method. This quantifies the growth rate's dependence on every interaction between the two subsystems. This directly gives the drift in the dominant eigenvalue caused by the global acceleration term, which couples the acoustics to the hydrodynamics, avoiding time-consuming nonlinear simulations [12]. The ultimate aim is to set up a robust framework for stability, receptivity and sensitivity analysis of combustion-acoustic systems and thereby to control thermo-acoustic instabilities by exploiting the behaviour of hydrodynamic instabilities.

2. Governing equations

The non-dimensional compressible continuity, momentum, and energy equations are

$$\frac{\partial \rho}{\partial \tau} + \left(\frac{L}{h}M\right) \nabla \cdot (\rho \mathbf{u}) = 0, \tag{1}$$

$$\rho \frac{\partial \mathbf{u}}{\partial \tau} + \left(\frac{L}{h}M\right) \Big[\rho \mathbf{u} \cdot \nabla \mathbf{u} + \frac{1}{\gamma M^2}\nabla p - \frac{1}{S_1 Re}\nabla \cdot \bar{\boldsymbol{\tau}}\Big] = 0, \tag{2}$$

$$\rho \frac{\partial T}{\partial \tau} + \left(\frac{L}{h}M\right) \Big[\rho \mathbf{u} \cdot \nabla T - \frac{1}{S_1 RePr}\Delta T - \rho Da Q_R + \frac{\gamma - 1}{\gamma}\mathbf{u} \cdot \nabla p\Big] + \frac{\gamma - 1}{\gamma}\frac{\partial p}{\partial \tau} = 0, \tag{3}$$

where ρ is the density scaled by the ambient (oxidizer) density, $\tilde{\rho}_0$; $\mathbf{u}$ is the velocity scaled by the inlet fuel velocity, $\tilde{u}_f$; p is the pressure scaled by the ambient pressure, $\tilde{p}_0$; T is the temperature non-dimensionalized as $(\tilde{T} - \tilde{T}_0)/(\tilde{T}_f - \tilde{T}_0)$, where $\tilde{T}_f$ is the adiabatic flame temperature and $\tilde{T}_0$ is the ambient oxidizer temperature; Q_R is the rate of heat released by reaction; M is the Mach number; γ is the heat capacity ratio; Re is the Reynolds number based on fuel parameters, $\tilde{\rho}_f \tilde{u}_f h/\tilde{\mu}$, with $\tilde{\mu}$ being the dynamic viscosity; S_1 is the oxidizer-to-fuel density ratio, $\tilde{\rho}_0/\tilde{\rho}_f$; Pr is the Prandtl number $\tilde{\mu}\tilde{c}_p/\tilde{\lambda}$, where $\tilde{c}_p$ is the heat capacity at constant pressure and $\tilde{\lambda}$ is the thermal conductivity; Da is the Damköhler number $(\gamma - 1)\,\tilde{\omega}_0 h/(\gamma \tilde{u}_0)$; $\tilde{\omega}_0$ is the reference reaction rate. We assume the Newtonian constitutive relation for the viscous stress tensor, $\bar{\boldsymbol{\tau}} = \nabla \mathbf{u} + (\nabla \mathbf{u})^T - 2/3\,(\nabla \cdot \mathbf{u})\,\mathbf{I}$, where $\mathbf{I}$ is the identity tensor. The reference length is the mean flame length, h, upstream of which it is assumed that most of the heat is released by chemical reaction. The flame acts on the acoustics as a compact heat source of finite spatial extent. The reference time is $L/\tilde{c}_0$, where $\tilde{c}_0$ is the reference speed of sound and L is the length of the combustor (Fig. 1). τ is the dimensionless acoustic time. We have neglected body forces and viscous dissipation effects in the energy equation, as a result of the low-Mach number limit. We have assumed Fourier's law for conduction, constant thermo-viscous properties, and a perfect gas law. We study diffusion flames with one-step chemistry by defining the mixture fraction, Z, and using the non-dimensional Arrhenius' law

$$\rho \frac{\partial Z}{\partial \tau} + \left(\frac{L}{h}M\right) \left[\rho \mathbf{u} \cdot \nabla Z - \frac{1}{S_1 ReSc}\Delta Z\right] = 0, \tag{4}$$

$$Q_R = \rho^2 \omega = \rho^2 \left[\left(Z - \frac{T}{s+1}\right)\left(1 - Z - \frac{sT}{s+1}\right) - \kappa T^2\right] \times \exp\left[\frac{-\beta\,(1-T)}{1 - \alpha\,(1-T)}\right], \tag{5}$$

where Sc is the Schmidt number; $\tilde{\mu}/(\tilde{\rho}_f \tilde{D})$, with $\tilde{D}$ being the mass diffusivity; s is the stoichiometric ratio; κ is the equilibrium constant; $\alpha = 1 - \tilde{T}_f/\tilde{T}_0$; β is the Zeldovich number, $\alpha \tilde{T}_a/\tilde{T}_0$, where $\tilde{T}_a$ is the activation energy; the Lewis number is assumed to be unity and $\tilde{\rho}\tilde{D}$ is constant. The state equation becomes $\rho\,[(\,S_1 - 1\,)Z + 1]\;[(\,S_2 - 1\,)T + 1] - p = 0$, where S_2 is the adiabatic-flame-to-ambient temperature ratio. These equations, with slightly different non-dimensionalization, were also used in [17, 18].

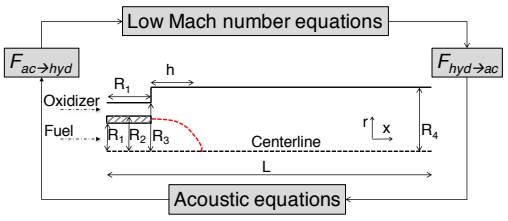

Figure 1: Coupling between combusting hydrodynamics, governed by the low-Mach number equations, and acoustics. Depending on the multiple-scale limit, the coupling terms, $F_{ac \to hyd}$ and $F_{hyd \to ac}$, have different expressions (table 1). The schematic shows the coaxial jet combustor. $R_1 = 3.157\ cm$, $R_2 = 3.175\ cm$, $R_3 = 4.685\ cm$, $R_4 = 6.115\ cm$, $L = 9R_1$. The curved dashed line represents the stoichiometric surface. In the computations, all the spatial variables are scaled by the fuel jet diameter, $2R_1$.

3. Two-way coupling of hydrodynamics and acoustics

We couple the reacting low-Mach number equations, which govern hydrodynamic phenomena, with the acoustic equations in a mathematically consistent manner by combining an asymptotic approach with a multiple-scale method. This enables us to reduce the complexity of the full problem governed by (1)-(5). In thermo-acoustics, multiple-scale methods were applied, among others, by Moeck et al. [11], Mariappan and Sujith [12], Balaji and Chakravarthy [13]. The two perturbation parameters are the Mach number, $M \sim O(\epsilon)$ and the flame compactness, $h/L \sim O(\epsilon^n)$, where $0 < \epsilon \ll 1$. The Mach number is the smallest perturbation parameter, hence $0 \leq n \leq 1$. In most gas turbine chambers, acoustic phenomena evolve at scales that are different from those of hydrodynamic phenomena. This is because low-frequency thermo-acoustic instabilities are expected to scale with the longitudinal length, L, whereas hydrodynamic instabilities are expected to scale with the flame length or shear-layer thickness, h. High-frequency transverse instabilities are not considered in this multiple-scale analysis. We define t as the hydrodynamic time, $\mathbf{x}$ as the hydrodynamic spatial coordinates, and $\boldsymbol{\xi}$ as the acoustic spatial coordinates. Observing that hydrodynamic phenomena scale with the convective time, $h/\tilde{u}_0$, and flame length, h; and acoustic phenomena scale with the acoustic time, $L/\tilde{c}_0$, and combustor's length, L, it follows that $t/\tau = ML/h = \epsilon^{1-n}$ and $x_i/\xi_i = L/h = \epsilon^{-n}$. Physically, this means that we require $\epsilon^{(n-1)} \geq 1$ acoustic time units, τ, to obtain one convective time unit, t. In such a case the acoustic time is faster than the convective time. Likewise, we require $\epsilon^n \leq 1$ acoustic spatial units, $\boldsymbol{\xi}$, to obtain one convective spatial unit, $\mathbf{x}$. In such a case the acoustic space is longer than the convective space. We show and discuss three multiple-scale limits.

(i) In the double-time-double-space limit (2T-2S), the acoustics evolve at shorter time scales and longer spatial scales than the hydrodynamics. The description of this approach is given by Balaji and Chakravarthy [13], who carried out nonlinear simulations of diffusion flames in a backward-facing step dump combustor. In this case $0 < n < 1$, i.e., the perturbation coefficient is strictly positive and smaller than unity.

(ii) In the double-time-single-space limit (2T-1S), the acoustics evolve at shorter time scales but at the same spatial scale as the hydrodynamics. The derivation is provided by Müller [19]. In this case $n = 0$, i.e., there are no different spatial scales.

(iii) In the single-time-double-space limit (1T-2S), the acoustics evolves at longer spatial scales but at the same time scale as the hydrodynamics. In this case $n = 1$, i.e., there are no different time scales. The derivation for non-reacting atmospheric flows is given by Klein [20]; for a one-dimensional acoustic system with a flame by Moeck et al. [11]; and for an electrical Rijke tube by Mariappan and Sujith [12].

3.1. Multiple-scale method

To reduce the complexity and separate out hydrodynamic and acoustic phenomena from the original equations (1)-(5), we carry out the following procedure.

(i) Asymptotic expansion: We expand the variables assuming a low-Mach number decomposition of the form $\phi = \sum_i \epsilon^i \phi_i$, where ϕ denotes a generic variable.

(ii) Differential operators decomposition: In the double-time-double-space approach (2T-2S), $\phi(\mathbf{x}, t) \rightarrow \phi(\mathbf{x}, \boldsymbol{\xi}, t, \tau)$. By applying the chain rule we decompose both the temporal and spatial derivatives as $\partial/\partial\tau \rightarrow \partial/\partial\tau + \epsilon^{1-n}\partial/\partial t$, and $\nabla \rightarrow \nabla_x + \epsilon^n \nabla_\xi$. In the double-time-single-space approach (2T-1S), $\phi(\mathbf{x}, t) \rightarrow \phi(\mathbf{x}, t, \tau)$ and only the temporal derivative is decomposed as $\partial/\partial\tau \rightarrow \partial/\partial\tau + \epsilon^{1-n}\partial/\partial t$. In the single-time-double-space approach (1T-2S), $\phi(\mathbf{x}, t) \rightarrow \phi(\mathbf{x}, \boldsymbol{\xi}, t)$ and only the spatial derivative is decomposed as $\nabla \rightarrow \nabla_x + \epsilon^n \nabla_\xi$.

(iii) Order-by-order matching: New equations are defined by collecting terms in order of ϵ.

(iv) Average-plus-fluctuation decomposition and equation averaging: In 2T-2S, the time decomposition $\phi = \langle\phi\rangle_\tau + \phi'^\tau$, is substituted into the operator presented in (ii) and the equations are time averaged over the slow hydrodynamic time scale t. The angle brackets $\langle\cdot\rangle_\tau$ represent the time average of the fast variable, τ, the superscript $'\tau$ represents the fluctuation over the fast time τ. Then, the variables are split as $\phi = \langle\phi\rangle_x + \phi'^x$, and the equations are spatially averaged over the long acoustic spatial scale $\boldsymbol{\xi}$. The angle brackets $\langle\cdot\rangle_x$ represent the spatial average of the short spatial variable $\mathbf{x}$, the superscript $'x$ represents the fluctuation over the short spatial scale $\mathbf{x}$. In 2T-1S, only the time decomposition and averaging is applied. In 1T-2S, only the spatial decomposition and averaging is applied.

Regardless of the limit used, the above four steps lead to a nonlinearly coupled set of low-Mach number and acoustic equations, which are explained in sections 3.2-3.3.

3.2. Hydrodynamic phenomena: the low-Mach number equations

Hydrodynamic phenomena are governed by the continuity, momentum, energy and mixture-fraction low-Mach number equations for constant pressure flames [21]

$$\frac{\partial \rho}{\partial t} + \nabla_x \cdot (\rho \mathbf{u}) = 0, \tag{6}$$

$$\frac{\partial \mathbf{u}}{\partial t} + \mathbf{u} \cdot \nabla_x \mathbf{u} + \frac{1}{\gamma \rho} \nabla_x p - \frac{1}{S_1 Re \rho} \nabla_x \cdot \bar{\boldsymbol{\tau}} = F_{ac \rightarrow hyd}, \tag{7}$$

$$\frac{\partial T}{\partial t} + \mathbf{u} \cdot \nabla_x T - \frac{1}{S_1 RePr \rho} \Delta_x T - DaQ_R = 0, \tag{8}$$

$$\frac{\partial Z}{\partial t} + \mathbf{u} \cdot \nabla_x Z - \frac{1}{S_1 ReSc \rho} \Delta_x Z = 0, \tag{9}$$

where the spatial gradient ∇_x acts on the hydrodynamic spatial scale, $\mathbf{x}$. The state equation is $\rho\,[(\,S_1 - 1\,)Z + 1]\,[(\,S_2 - 1\,)T + 1] = 1$, which shows that the thermodynamic pressure is constant and equal to unity when non-dimensionalized. This nonlinear problem can be conveniently expressed in matrix form as $\dot{\mathbf{q}}_{hyd} - \mathbf{H}(\mathbf{q}_{hyd}) = \mathbf{F}\,(\mathbf{q})_{ac \rightarrow hyd}$, where $\mathbf{q}_{hyd} = (\rho, \mathbf{u}, T, Z)^T$ is the vector of the hydrodynamic variables; $\dot{\mathbf{q}}_{hyd} = \partial \mathbf{q}_{hyd}/\partial t$; $\mathbf{q} = (\mathbf{q}_{hyd}, \mathbf{q}_{ac})^T$, with $\mathbf{q}_{ac}$ being the vector of the acoustic variables (section 3.3); and $\mathbf{F}_{ac \rightarrow hyd} = (0, F_{ac \rightarrow hyd}, 0, 0)^T$ is the vector of forcing terms (table 1). The hydrodynamic operator, $\mathbf{H}$, is nonlinear because of the convective derivatives and reaction term.

	2T-2S	2T-1S	1T-2S
$F_{hyd\to ac_{con}}$	$-\nabla_\xi \cdot \left(\langle \rho \rangle_x \left\langle \mathbf{u}^{'\tau} \right\rangle_x + \left\langle \rho^{'x} \mathbf{u}^{'x} \right\rangle_x \right)$	0	$-\nabla_\xi \cdot \left(\left\langle \rho^{'x} \mathbf{u}^{'x} \right\rangle_x \right)$
$F_{hyd\to ac_{mom}}$	0	0	$-1/\langle \rho \rangle_x \, \partial/\partial t \left\langle \rho^{'x} \mathbf{u}^{'x} \right\rangle_x$
$F_{hyd\to ac_{en}}$	$-\gamma \langle \nabla_\xi \cdot \mathbf{u} \rangle_x$	DaQ'_{R0}	$Da \langle Q_{R1} \rangle_x$
$F_{ac\to hyd}$	$-1/\rho \nabla_x \cdot \left\langle \rho \mathbf{u}^{'\tau} \otimes \mathbf{u}^{'\tau} \right\rangle_\tau$	$-1/\rho \nabla_x \cdot \left\langle \rho \mathbf{u}^{'\tau} \otimes \mathbf{u}^{'\tau} \right\rangle_\tau$	$-1/(\gamma\rho) \nabla_\xi p^{'\tau}$

Table 1: Terms coupling hydrodynamics to acoustics, *hyd* $\to$ *ac*, and acoustics to hydrodynamics, *ac* $\to$ *hyd*. These terms depend on the multiple-scale limit: Double-time-double-space (2T-2S), double-time-single-space (2T-1S) and single-time-double-space (1T-2S). In 2T-1S $\mathbf{x} = \boldsymbol{\xi}$, in 1T-2S $t = \tau$. The numeric subscripts of Q_{R0} and Q_{R1} refer to the orders of the heat-release asymptotic expansion.

3.3. Acoustic phenomena

The acoustic variables are governed by the continuity, momentum and energy equations

$$\frac{\partial \rho^{'\tau}}{\partial \tau} + \nabla_\xi \cdot \left(\langle \rho \rangle_x \, \mathbf{u}^{'\tau} \right) = F_{hyd\to ac_{con}}, \tag{10}$$

$$\frac{\partial \mathbf{u}^{'\tau}}{\partial \tau} + \frac{1}{\gamma \langle \rho \rangle_x} \nabla_\xi p^{'\tau} = F_{hyd\to ac_{mom}}, \tag{11}$$

$$\frac{\partial p^{'\tau}}{\partial \tau} + \gamma \nabla_\xi \cdot \mathbf{u}^{'\tau} = F_{hyd\to ac_{en}}, \tag{12}$$

where the spatial gradient ∇_ξ acts on the acoustic spatial scale, $\boldsymbol{\xi}$. This problem can be expressed as $\dot{\mathbf{q}}_{ac} - \mathbf{A}\mathbf{q}_{ac} = \mathbf{F}(\mathbf{q})_{hyd\to ac}$, where $\mathbf{q}_{ac} = (\rho^{'\tau}, \mathbf{u}^{'\tau}, p^{'\tau})^T$ is the vector of the acoustic variables; $\dot{\mathbf{q}}_{ac} = \partial \mathbf{q}_{ac}/\partial\tau$; and $\mathbf{F}_{hyd\to ac} = \left(F_{hyd\to ac_{con}}, F_{hyd\to ac_{mom}}, F_{hyd\to ac_{en}} \right)^T$ is the vector of forcing terms. The acoustic operator, $\mathbf{A}$, is linear. The nonlinearities are contained in the forcing term. State and mixture fraction equations (not shown) are required for the calculation of the heat-release terms in 2T-1S and 1T-2S (section 3.4).

The acoustics dissipates mainly by radiation from the combustor's open boundaries and slightly in the viscous-thermal boundary layer. Nonlinear damping effects, such as vortex roll-up at sharp changes to the cross-sectional area, are not included in the current study because this study focuses on the stability of infinitesimal perturbations. In this asymptotic analysis, acoustic dissipation in the viscous-thermal boundary layer is neglected because it is of higher order. Physically, the acoustic viscous terms are negligible because (i) when the acoustic time is faster than the hydrodynamic time, the acoustic Reynolds number is very large and (ii) when the acoustic scale is longer than the hydrodynamics, the boundary layer scale is negligible. However, near the wall, these terms may be important and need modelling. Therefore, the viscous-thermal acoustic dissipation is modelled as a sink term in the acoustic energy equation proportional to p'^{τ}, in a similar manner to [13]. The acoustic radiation should be modelled by impedance boundary conditions, which makes the final eigenproblem nonlinear in the eigenvalue [6]. Although the methods presented here can be applied to nonlinear eigenproblems [22], this is beyond the scope of this paper, therefore, ideal open ends are assumed, making the eigenproblem linear.

3.4. Coupling terms

The terms coupling the hydrodynamics to the acoustics depend on the multiple-scale limit considered (table 1). For a more exhaustive physical understanding of these terms, Lighthill's analogies could be used, although this is not attempted here. Here, we comment on the terms that are most relevant to thermo-acoustics.

On the one hand, the hydrodynamics is an acoustic energy source through the spatially averaged dilation of the flow in the 2T-2S limit, which acts as a dipole-like source. This tends to the classic unsteady heat release in the 2T-1S and 1T-2S limits, which acts as a monopole-like source (second to last row in table 1). Physically, the unsteady heat release only partly contributes to the acoustic energy input in the 2T-2S limit. (The unsteady heat release is calculated by using the acoustic density, temperature and mixture-fraction equations.) On the other hand, the acoustics forces the hydrodynamic momentum via the nonlinear term $-1/\rho\,\nabla_x \cdot \langle \rho \mathbf{u}^{'\tau} \otimes \mathbf{u}^{'\tau} \rangle_\tau$ in the double space limits (2T-2S and 1T-2S, last row in table 1). This term is known as the acoustic Reynolds stress [23], which, as opposed to the turbulent Reynolds stress, does not require closure because it is obtained from the acoustic solver. In the 1T-2S limit, the hydrodynamic momentum is forced through the acoustic pressure gradient that imposes a global acceleration.

In compact form, the coupled thermo-acoustic problem (Fig. 1), governed by (6)-(12), reads

$$\dot{\mathbf{q}} - \mathbf{T}\left(\mathbf{q}\right) = \mathbf{F}, \tag{13}$$

where $\mathbf{T}\left(\mathbf{q}\right)$ is the nonlinear thermo-acoustic operator, and $\mathbf{F} = \left(\mathbf{F}_{ac\rightarrow hyd},\, \mathbf{F}_{hyd\rightarrow ac}\right)^T$.

4. Linearization, stability and intrinsic sensitivity

In linearization, we typically assume that the amplitudes of the hydrodynamic variables are $\sim O(1)$ and those of the acoustic variables are $\sim O(\varepsilon)$. (This perturbation parameter ε has nothing to do with the multiple-scale perturbation parameter ϵ.) Physically, we regard the acoustics as a perturbation field on top of the hydrodynamic flow. However, we show that different multiple-scale limits cause different linear behaviours. The hydrodynamic variables are split as $\mathbf{q}_{hyd} = \bar{\mathbf{q}}_{hyd} + \varepsilon \mathbf{q}_{hyd,1}$, where $\bar{\mathbf{q}}_{hyd} \sim O(1)$ is the steady mean flow calculated from numerical simulations or experiments and $\varepsilon \mathbf{q}_{hyd,1}$ is the low-frequency large-scale organized motion. Therefore, the perturbation hydrodynamic vector, $\mathbf{q}_{hyd,1}$, and acoustic vector, $\mathbf{q}_{ac}$, are of the same order ε but act at different scales. When linearized, the thermo-acoustic problem can be expressed in compact form as $\dot{\mathbf{q}} = \mathbf{J}\mathbf{q}$, where

$$\mathbf{J} = \begin{bmatrix} \left(\frac{\delta \mathbf{H}}{\delta \mathbf{q}_{hyd}} + \frac{\delta \mathbf{F}_{ac\rightarrow hyd}}{\delta \mathbf{q}_{hyd}}\right) & \frac{\delta \mathbf{F}_{ac\rightarrow hyd}}{\delta \mathbf{q}_{ac}} \\ \frac{\delta \mathbf{F}_{hyd\rightarrow ac}}{\delta \mathbf{q}_{hyd}} & \left(\mathbf{A} + \frac{\delta \mathbf{F}_{hyd\rightarrow ac}}{\delta \mathbf{q}_{ac}}\right) \end{bmatrix}. \tag{14}$$

The Jacobian operator is the functional derivative of the thermo-acoustic operator, $\mathbf{J} = \delta\mathbf{T}/\delta\mathbf{q}$, and is evaluated at the base flow $\bar{\mathbf{q}}_{hyd}$. When we linearize the double-time limits, 2T-2S and 2T-1S, the acoustic Reynolds stress, which is the term coupling the acoustics to the hydrodynamics, vanishes. The linear dynamics is only one-way coupled because the coupling term $\delta\mathbf{F}_{ac\rightarrow hyd} = O(\varepsilon^2)$ is negligible in (14). This is because, when there are two time scales (the acoustic time being faster than the convective time), the acoustics are driven by the hydrodynamics but do not affect it. Physically, this is because the influence of the acoustics averages to zero over the long time scale of the hydrodynamics. This is equivalent to one of the mechanisms described in [1] in which, if one considers perturbations convecting at uniform speed along a long flame such that there are many oscillations along the flame, most of the heat release perturbations cancel out, causing the flame to behave as a low pass filter. From this two-scale argument, a thermo-acoustic oscillation is more likely to exist when the time scales are the same. In a classic picture of a thermo-acoustic instability, the two time scales are indeed the same [12]. In fact, when only one time scale is modelled, as in 1T-2S, the thermo-acoustic system is two-way *linearly* coupled because $\delta\mathbf{F}_{ac\rightarrow hyd} = O(\varepsilon)$, i.e., there is a non-trivial interaction between hydrodynamic and thermo-acoustic stability, as shown in section 5. Therefore, we use the 1T-2S limit from now on. By using modal transformations, $\mathbf{q}_1 = \hat{\mathbf{q}}\exp(\sigma t)$, the resulting direct

thermo-acoustic eigenproblem becomes $\sigma\hat{\mathbf{q}} = \mathbf{J}\hat{\mathbf{q}}$, where σ is the complex eigenvalue. The adjoint modal transformation, $\mathbf{q}_1^+ = \hat{\mathbf{q}}^+ \exp(-\sigma^* t)$, yields the adjoint eigenproblem $\sigma^*\hat{\mathbf{q}}^+ = \mathbf{J}^H\hat{\mathbf{q}}^+$, where * is the complex conjugate and ^{H} denotes the complex transpose. The adjoint eigenfunctions provide the receptivity to open-loop forcing. For example, the most receptive zone due to flow velocity disturbances is the shear-layer where the two streams mix [24].

The eigenfunctions and their adjoints can be combined to predict the first-order eigenvalue-drift caused by a spatially localized perturbation to the system, $\delta\mathbf{J}$, as

$$\delta\sigma = \hat{\mathrm{q}}_i^{+H}\delta\mathrm{J}_{ij}\hat{\mathrm{q}}_j, \tag{15}$$

where the indices denote the components of the matrix/vector arrangement of the continuous operators, i.e. $i, j = \rho, \mathbf{u}, T, Z, \rho^{'\tau}, \mathbf{u}^{'\tau}, p^{'\tau}$. The eigenfunctions are normalized such that $\hat{\mathbf{q}}^{+H}\hat{\mathbf{q}} = 1$. Equation (15) was introduced in thermo-acoustics to calculate the effect of external feedback mechanisms, such as a hot wire, and design-parameter changes, such as the flame inlet geometric ratio, in the stability [7, 8, 9] via appropriate models for the thermo-acoustic perturbation $\delta\mathbf{J}$. We introduce the concept of *intrinsic sensitivity*, extending the structural sensitivity used in [7, 18], defined as the eigenvalue's sensitivity to intrinsic physical mechanisms. Here, the perturbation operator of the eigenvalue's sensitivity formula (15) is the Jacobian itself, i.e., $\delta\mathbf{J} = \varepsilon\mathbf{J}$. This enables us to identify the regions of the flow where the hydrodynamic and acoustic subsystems are active and quantify how they affect the overall thermo-acoustic stability. When the flow is laminar, the real part of (15) provides a map showing the regions to which the thermo-acoustic stability is most sensitive to the j-th variable through the i-th equation. Likewise, the imaginary part of (15) shows the regions to which the thermo-acoustic angular frequency is most sensitive.

5. Application to a coaxial jet combustor

We use the 1T-2S limit because it enables the two-way linear coupling between the hydrodynamic and acoustic subsystems. The problem is cast in weak form in cylindrical coordinates and Fourier-transformed in the azimuthal direction exploiting the axisymmetry. We discretize the equations with a finite element method (`http://www.freefem.org/ff++/`) and solve the eigenproblem and its adjoints with a shift-invert method with ARPACK (`http://www.caam.rice.edu/software/ARPACK/`). We use a Discrete Adjoint approach [7, 25] to ensure that the adjoint spectra match the complex conjugate of the direct spectra to machine precision. The code was validated against the solutions of [18] and the spectra matched with an error smaller than 0.5%. To test our method, we use the coaxial jet combustor of [14, 15], which is schematically shown in Fig. 1. The mean flow has no swirl and we investigate the azimuthally symmetric (non-spiralling) Fourier component, whose hydrodynamic mode can couple with longitudinal acoustic oscillations creating a thermo-acoustic instability. The mean-flow boundary conditions are plug-flow at the inlet, no-slip flow at the walls and convective outflow at the outlet. As for the stability equations, homogeneous Dirichlet boundary conditions are prescribed on the low-Mach number equations everywhere except for the outlet, where homogeneous Neumann conditions are imposed. The acoustic pressure is zero at the ends (open-ended combustor) and the acoustic velocity is zero at the rigid walls. After performing convergence tests, we choose a discretization with 90,429 triangles and 45,792 vertices for both the hydrodynamics and acoustics. The case presented has the following parameters: $Re = 100$ (laminar flow and steady solution); $Pr = Sc = 0.7$; $\kappa = 0.01$; $s = 2$; $\beta = 3$; $S_1 = 7$; $S_2 = 6$; $Da = 10^6$. These conditions correspond to a methane/air flame. A similar flame was studied by [17] in an unconfined domain without inlets. In this laminar case, the mean flow (Fig. 2) is a steady solution of the governing equations (6)-(9) and it is labelled the *base flow*. The base flow is obtained by time-marching a structured Large-Eddy Simulation low-Mach number code [15] until the steady solution is obtained. The chemistry is solved with a Flamelet Progress Variable Method [15].

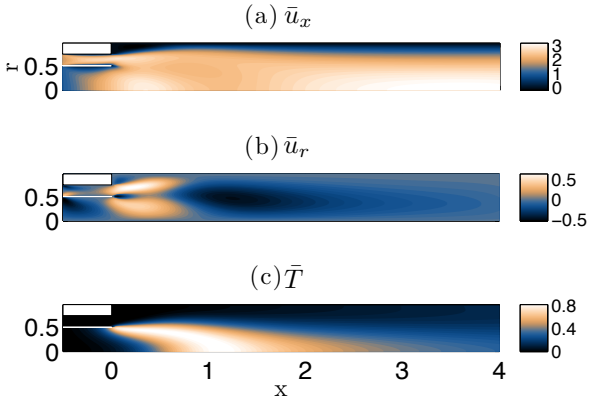

Figure 2: Base-flow (a) axial velocity, (b) radial velocity and (c) temperature.

On the one hand, the combusting hydrodynamic flow, when the coupling forcing terms are set to zero, is globally stable. The dominant eigenvalue is $\sigma = -0.100 + \mathrm{i}1.041$. The radial velocity and temperature eigenfunctions are depicted in Fig. 3a,b, respectively. On the other hand, the acoustics, when the linearized low-Mach number flow is not coupled through forcing terms, are stable because of the acoustic damping, although close to neutral stability. The eigenvalue is $\sigma = -0.00031 + \mathrm{i}0.630$. As a check, the non-dimensional acoustic angular frequency $\sigma_i = 0.630$ is close to the non-dimensionalized first duct resonance, $(2\pi\tilde{c}_0/2L)/(\tilde{c}_0/2R_1) = 0.698$, where $L = 9R_1$ is the combustor's length (Fig. 1). The acoustic mode is longitudinal (Fig. 3c), although the effect of the radial acoustic motion is not negligible at the inlet (Fig. 3d).

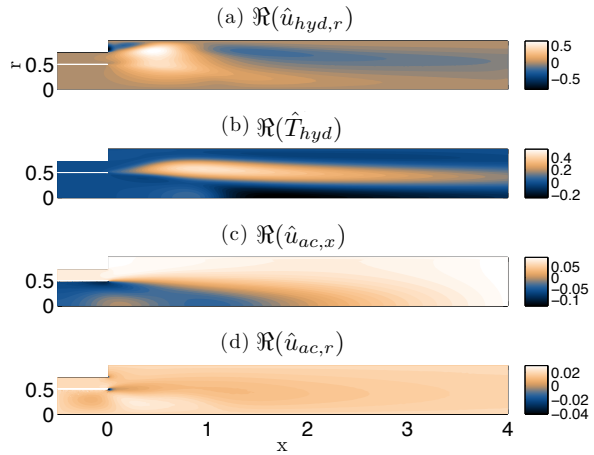

Figure 3: Real part of (a,b) hydrodynamic and (c,d) acoustic eigenfunctions.

When two-way coupled, the low-Mach number flow and acoustics become unstable, with dominant eigenvalue $\sigma = 0.102 + \mathrm{i}0.731$. The angular frequency is close to the acoustic frequency; the instability is driven

by acoustic effects because the unstable mode is primarily acoustic. In this stability framework, the hydrodynamics is simulated and interacts with the acoustics. This overcomes the limitations of simple thermo-acoustic models, in which all the information from the hydrodynamics is typically encapsulated in response functions [4, 5], $n-\tau$ models and other models for the flame convective speed [1].

We can study the effect that the acoustics has on the hydrodynamic stability, which is *exactly* given by the intrinsic sensitivity map $\delta\sigma/\varepsilon = \hat{\mathbf{q}}_{hyd}^{+H}\mathbf{J}_{12}\hat{\mathbf{q}}_{ac}$. This is a spatial function and $\mathbf{J}_{12}$ is the coupling operator from the acoustics to the hydrodynamics (top-right component of the matrix (14)) through the acoustic pressure gradient (bottom-right term in table 1). This formula quantifies how much a small perturbation to the acoustic field $\sim \varepsilon\mathbf{J}_{12}\hat{\mathbf{q}}_{ac}$ changes the thermo-acoustic eigenvalue of the coupled system through hydrodynamic physical process ($\hat{\mathbf{q}}_{hyd}^{+H}$). The real part of this quantity is shown in Fig. 4a. We note that the highest sensitivity straddles the recirculation region at the top left corner. The acoustics is acting as an extra feedback momentum source, enhancing the hydrodynamic sensitivity, which is, indeed, often close to the recirculation boundary [25]. (From a hydrodynamic standpoint, in the 1T-2S linear limit, the acoustics cannot be viewed as an external forcing.) Changes in the strength of the coupling from the acoustics to the hydrodynamics here will have the most influence on this mode, i.e., the mode is very sensitive to the coupling in this region. However, this is only one component of the intrinsic sensitivity and the coupling from acoustics to hydrodynamics is not the dominant mechanism. The maximum growth rate drift is $\delta\sigma_r \sim O(10^{-4})$.

Following the same line of reasoning, we study the effect that the hydrodynamics has on the stability through acoustic mechanisms, whose intrinsic sensitivity is $\delta\sigma/\varepsilon = \hat{\mathbf{q}}_{ac}^{+H}\mathbf{J}_{21}\hat{\mathbf{q}}_{hyd}$, where $\mathbf{J}_{21}$ is the coupling term from the hydrodynamics to the acoustics (bottom-left component of the matrix (14)). This formula quantifies how much a small perturbation to the hydrodynamic field $\sim \varepsilon\mathbf{J}_{21}\hat{\mathbf{q}}_{hyd}$ changes the thermo-acoustic eigenvalue of the coupled system through acoustic physical process ($\hat{\mathbf{q}}_{ac}^{+H}$). This map is depicted in Fig. 4b. The maximum value is $\delta\sigma_r \sim O(10^{-2})$. The region of high sensitivity straddles the stoichiometric line, where most of the heat is released by the flame. This shows that a small change in the coupling from hydrodynamics to acoustics causes a larger stability drift, i.e. $\delta\sigma_r \sim O(10^{-2})$, than a small change in the coupling from the acoustics to the hydrodynamics, i.e. $\delta\sigma_r \sim O(10^{-4})$. In other words, small changes of the strength of the hydrodynamic feedback (i.e., coupling) greatly change the flame response to acoustic perturbations which, in turn, have significant influence on the thermo-acoustic stability. In the limit of classic one-way coupled thermo-acoustic models, this result is consistent with the diffusion-flame structural sensitivity and Rayleigh Index analysis of [8]. In this paper, we have focused on the terms coupling the hydrodynamics to the acoustic energy equation because they are directly connected to the unsteady heat release. The investigation of the remaining coupling terms in the acoustic continuity and momentum equations (table 1) is left for future studies. This can be directly tackled with the intrinsic structural sensitivity concept introduced in Eq. (15).

5.1. Effect of the global acceleration term

In the Rijke-tube configuration of [12], the coupling term $F_{ac\to hyd}$, also known as the global acceleration term [11, 12], was shown to have a noticeable destabilizing effect on the thermo-acoustic stability. In our configuration, as the coupling strength from the acoustics to the hydrodynamics increases, the growth rate decreases non-monotonically (Fig. 5a). This is physically explained via the Rayleigh Criterion [2]. By substituting the acoustic eigenfunctions into the definition of acoustic energy, E_{ac}, and neglecting damping to a first approximation [8], the acoustic-energy rate of change is given by the integral of the Rayleigh Index over the acoustic domain, $\sigma_r E_{ac} = 1/4\Re\left(\int_V \hat{p}'^{\tau *}\hat{\mathcal{Q}}\mathrm{d}\boldsymbol{\xi}\right)$; where $\hat{\mathcal{Q}}$ is the acoustic heat release given by $F_{hyd\to ac_{en}}$ in table 1. Both $\hat{p}'^{\tau}$ and $\hat{\mathcal{Q}}$ are implicit function of the global acceleration term $F_{ac\to hyd}$, and so

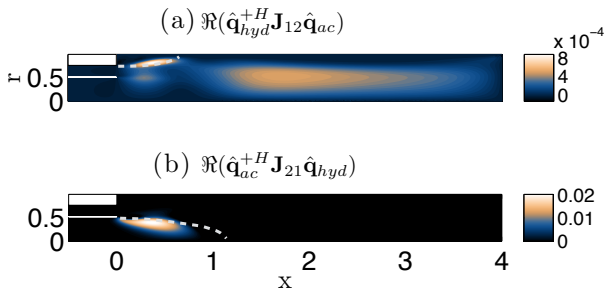

Figure 4: Growth-rate sensitivity (a) to intrinsic hydrodynamic feedback feeding the momentum equation, the maximum straddles the recirculation-boundary (upper dashed line) and (b) sensitivity to the hydrodynamics through acoustic mechanisms, the maximum straddles the stoichiometric line (lower dashed line).

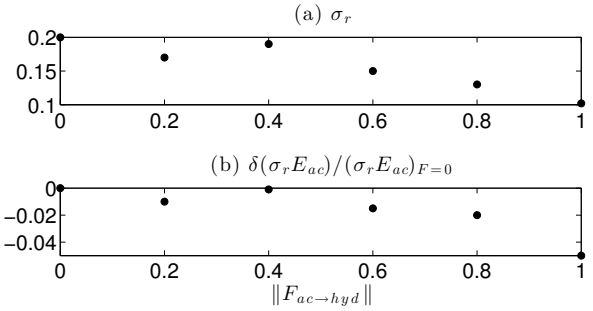

Figure 5: Effect of the coupling term $F_{ac\to hyd}$ on (a) the thermo-acoustic growth rate and (b) Rayleigh Criterion as a function of its normalized strength.

is $\sigma_r E_{ac}$. By splitting the contribution as $\sigma_r E_{ac} = (\sigma_r E_{ac})_{F=0} + \delta(\sigma_r E_{ac})$, where the subscript $F = 0$ is the contribution when $\|F_{ac\to hyd}\| = 0$ and $\delta(\cdot)$ is the contribution when $\|F_{ac\to hyd}\| > 0$, we see that the effect that the global acceleration term has on the thermo-acoustic stability depends on the phase of $\delta(\hat{p}'^{\tau *}\hat{\mathcal{Q}})$. In our configuration this is negative (Fig. 5b), i.e., the acoustic-energy rate of change decreases, whereas we expect that in [12] this energy excess was positive. We infer that, in general, the global acceleration term can have either a stabilizing or destabilizing effect because the feedback can be positive or negative depending on the phase (the eigenmodes are complex), which, in turn, depends on the configuration.

6. Conclusions

In the first part of this paper, we propose a methodology to calculate thermo-acoustic stability and sensitivity. By using different time and spatial scales for hydrodynamic and acoustic phenomena, we formulate a three-dimensional thermo-acoustic stability model in which the hydrodynamic field two-way interacts with the acoustics. Only a low-Mach number solver and an acoustic solver are needed. Three multiple scale limits are revisited and the two-way coupled system is linearized for stability analysis. It is shown that only when the acoustics evolve at larger spatial scales than the hydrodynamics but at the same time scale (1T-2S limit),

the linearized mutual interaction is two-way coupled. Using this limit, we define an eigenproblem and show how to study the sensitivity of the stability with an adjoint method. The *intrinsic sensitivity* identifies the regions and quantifies the effect that different subsystems have on the overall stability, which is suitable for multi-physical problems such as thermo-acoustics. In the second part, we apply this methodology to a coaxial jet combustor. We show that, although the hydrodynamic and acoustic subsystems are stable if considered separately, they become unstable when coupled together. The exact effect that the acoustics has on the hydrodynamic stability is quantified and physically interpreted as an extra momentum source enhancing the region of high hydrodynamic sensitivity. The hydrodynamics greatly influences the overall thermo-acoustic stability in regions of large heat release. The term coupling the acoustics to the hydrodynamics, known as the global acceleration term, can have either a stabilizing effect, as shown here, or a destabilizing effect, as shown in [12], on the thermo-acoustic stability. It was shown that this behaviour is due to its contribution to the Rayleigh Criterion, which is not a monotonic function of the global-acceleration strength.

This study shows that the relatively cheap combination of a low-Mach number solver, an acoustics solver, and adjoint sensitivity analysis can (i) avoid fully compressible calculations and (ii) reveal the most influential intrinsic mechanisms in thermo-acoustic instability. This technique can readily be extended to more complex geometries and passive control.

Acknowledgements The following sources of funding are gratefully acknowledged: the 2014 CTR Summer Program, ERC Project ALORS 2590620 and NASA grant #NNX10CF79P. L.M. also acknowledges the Royal Academy of Engineering Research Fellowships scheme. L.M. is grateful to Dr. C. Balaji and Prof. S.R. Chakravarthy for helpful discussions.

References

[1] T. Lieuwen, Unsteady Combustor Physics, Cambridge University Press, 2012.

[2] Lord Rayleigh, Nature 18, 1878, 319–321.

[3] S. R. Chakravarthy, O. J. Shreenivasan, B. Boehm, A. Dreizler, J. Janicka, J. Acoust. Soc. Am. 122 (1), 2007, 120–127.

[4] W. Polifke, A. Poncet, C. O. Paschereit, K. Döbbeling, J. Sound Vib. 245 (3), 2001, 483–510.

[5] N. Noiray, D. Durox, T. Schuller, S. Candel, J. Fluid Mech. 615, 2008, 139–167.

[6] F. Nicoud, L. Benoit, C. Sensiau, T. Poinsot, AIAA J. 45 (2), 2007, 426–441.

[7] L. Magri, M. P. Juniper, J. Fluid Mech. 719, 2013, 183–202.

[8] L. Magri, M. P. Juniper, J. Fluid Mech. 752, 2014, 237–265.

[9] L. Magri, M. P. Juniper, Int. J. Spray Combust. Dyn. 6 (3), 2014, 225–246.

[10] G. Rigas, N. P. Jamieson, L. K. B. Li, M. P. Juniper, J. Fluid Mech. 787, 2016, R1.

[11] J. P. Moeck, M. Oevermann, R. Klein, C. O. Paschereit, H. Schmidt, Proc. Combust. Inst. 32 (1), 2009, 1199–1207.

[12] S. Mariappan, R. I. Sujith, J. Fluid Mech. 680, 2011, 511–533.

[13] C. Balaji, S. R. Chakravarthy, in: 18th Int. Congr. Sound Vib., July, 2011.

[14] F. K. Owen, L. J. Spadaccini, C. T. Bowman, Proc. Combust. Inst. 16 (1), 1977, 105–117.

[15] C. D. Pierce, P. Moin, J. Fluid Mech. 504, 2004, 73–97.

[16] L. Magri, Y. C. See, M. Ihme, M. P. Juniper, in: Cent. Turbul. Res. Summer Progr., 199–208, 2014.

[17] J. W. Nichols, P. J. Schmid, J. Fluid Mech. 609, 2008, 275–284.

[18] U. A. Qadri, G. J. Chandler, M. P. Juniper, J. Fluid Mech. 775, 2015, 201–222.

[19] B. Müller, J. Eng. Math. 34, 1998, 97–109.

[20] R. Klein, ESAIM Math. Model. Numer. Anal. 39 (3), 2005, 537–559.

[21] T. Poinsot, D. Veynante, Theoretical and numerical combustion, 2nd ed., R. T. Edwards, 2005.

[22] M. P. Juniper, L. Magri, M. Bauerheim, F. Nicoud, in: Cent. Turbul. Res. Summer Progr., 189–198, 2014.

[23] J. Lighthill, J. Sound Vib. 61 (3), 1978, 391–418.

[24] B. Emerson, T. Lieuwen, M. P. Juniper, J. Fluid Mech. 788, 2016, 549–575.

[25] P. Luchini, A. Bottaro, Annu. Rev. Fluid Mech. 46, 2014, 1–30.